KIDNEY SEGMENTATION IN MRI SEQUENCES USING TEMPORAL DYNAMICS

Ying Sun[1], José M. F. Moura[1], Dewen Yang[2], Qing Ye[2], and Chien Ho[2]

[1]Department of Electrical and Computer Engineering
[2]Department of Biological Sciences, Carnegie Mellon University, PA 15213

ABSTRACT

We propose an energy-based image segmentation algorithm that uses the correlation information among pixels in the same image as well as the temporal correlation across the images in the sequence. We focus on MRI sequences that are extremely difficult to segment on the basis of single images. Our method detects motion-free objects whose intensities change across the image sequence. We introduce an energy functional that exploits the difference in the dynamics of the temporal signals associated with distinct pixels. We develop a level set approach and a region-growing algorithm to minimize the energy functional. Our tests in a transplantation study show that we successfully extract automatically the kidneys and their structures in magnetic resonance (MR) image sequences.

1. INTRODUCTION

We develop signal and image processing algorithms for non-invasive magnetic resonance imaging (MRI)-based methods to detect early rejection in organ transplantation. Our algorithms study the time variation pattern of the concentration of dextran-coated ultra-small superparamagnetic iron oxide (USPIO) particles after injection in the recipients. We study kidney transplantation with Brown Norwegian (BN) and D Agouti (DA) rats. We focus on isograft rats (BN→BN) and allograft rats (DA→BN). The time history of the MRI intensity at each pixel is the renal perfusion signal. We have developed in [1] and [2] a methodology that detects rejection by recognizing when the renal perfusion signals on transplanted kidneys are significantly distinct from the perfusion signals on native kidneys. Our method has produced so far encouraging results. In our previous study, the pixel selection was carried out manually across the MRI sequence by a human expert. This limits the selection to just a few pixels. There are a number of reasons why it is important to track the perfusion signals over as many pixels as possible: (1) studying only a few pixels raises risks similar to biopsies—early rejection may occur in localized spots that may be easily missed when undersampling the kidney; (2) a larger number of pixels provides a needed statistical significance in face of the appreciable variability of the MRI signals; and (3) tracking the perfusion signal across an MRI sequence requires that the same pixel be identified across the images in the sequence, a challenge that is a source of errors. We present our work on automating the process of pixel selection.

In dynamic MR kidney image sequences, it is particularly challenging to segment the kidney from its surrounding soft tissues and other organs. To use all the information available, we propose a new segmentation method that uses not only the spatial information provided by each single image in the MRI sequence but also the temporal information available, in particular, the perfusion signal. Ours is an energy minimization type approach [3], see section 2: we expand the energy functional to include space and time (the whole MRI sequence), see [4], and modify the energy terms to account for the spatial and temporal correlations. Our energy functional discerns among different regions in the MRI sequence by using a geometric inspired approach. It determines how close or distinct perfusion signal patterns are from their degree of similarity or dissimilarity as evaluated by a subspace distance—the gap metric [5]. We segment the MRI sequence by minimizing the energy functional through a level set-based approach [6] that we develop in section 2. Our experimental results show that by exploiting both the temporal and spatial information this method successfully segments the kidneys from other structures.

The paper is as follows. In section 2, we describe our energy functional and the level set Minimization algorithm. Section 3 describes the data and the preprocessing needed to successfully apply the approach in section 2. Section 4 presents our experimental results and concludes the paper.

2. ENERGY MINIMIZATION

Figure 1 displays 5 MR images sampled from the entire image sequence of a BN rat. Besides the kidneys, the images also display muscles, blood vessels, and other

This work was supported by grants from NIH grant (P41RR-03631 and R01RR/AI-15187).

0-7803-7584-X/02/$17.00 ©2002 IEEE

organs. It is difficult to distinguish from the images the different anatomical structures. Figure 2 illustrates the perfusion signals of 3 pixels across the image sequence respectively located at the cortex, medulla, and muscle. Here, we normalize the perfusion signal with respect to the intensity at the same pixel in the first frame. These dynamic sequences are all quite distinct; for instance, the intensity of the cortex pixel shows pronounced oscillations, whereas the intensity of the muscle pixel is very much noise like. This suggests that we can distinguish between the kidney and other anatomical structures based on their temporal responses. To quantify this dissimilarity, we introduce a metric that characterizes the distance between two dynamic signals.

Subspace distance Let $I_n(x,y)$, $n = 1,\ldots,N$, be the intensity at pixel (x,y) in MRI frame n, and N the number of frames in the MRI sequence. As we are interested in the temporal dynamics, we remove the mean from the perfusion signal and then collect this mean removed signal at each pixel (x,y) in the vector

$$\mathbf{I}(x,y) = [I_1(x,y) - \bar{I}(x,y), \ldots, I_n(x,y) - \bar{I}(x,y)].$$

where $\bar{I}(x,y) = \sum_{n=1}^{N} I_n(x,y)/N$. Vector $\mathbf{I}(x,y)$ is a 1-dimensional subspace in an N-dimensional space $\mathbb{R}^N$. The distance between two general subspaces $\mathbf{S}_1$ and $\mathbf{S}_2$ is given by the gap metric [5]

$$\mathrm{dis}\,(\mathbf{S}_1, \mathbf{S}_2) = \| \mathbf{P}_1 - \mathbf{P}_2 \|_2, \tag{1}$$

where $\mathbf{P}_1$ and $\mathbf{P}_2$ are the orthogonal projections onto the subspaces $\mathbf{S}_1$ and $\mathbf{S}_2$, respectively. In the simple case where the vector spaces are 1-dimensional, i.e., the vectors $\mathbf{v}_1$ and $\mathbf{v}_2$, the gap metric is simply

$$\mathrm{dis}\,(\mathbf{v}_1, \mathbf{v}_2) = |\sin\theta| \tag{2}$$

given by the magnitude of the sine of the angle θ between the two vectors. Instead of θ, we use $\frac{\theta}{2}$ to distinguish between $\sin\theta$ and $\sin(\pi - \theta)$. We define the distance function as

$$\mathrm{dis}^2\,(\mathbf{v}_1, \mathbf{v}_2) = \sin^2\frac{\theta}{2} = \frac{1-\cos\theta}{2} \tag{3}$$

where $\cos\theta$ is the correlation coefficient $c(\mathbf{v}_1, \mathbf{v}_2)$:

$$\cos\theta = c(\mathbf{v}_1, \mathbf{v}_2) = \frac{\langle \mathbf{v}_1, \mathbf{v}_2 \rangle}{\| \mathbf{v}_1 \|_2 \ \| \mathbf{v}_2 \|_2}, \tag{4}$$

with $\langle\cdot\rangle$ denoting the inner product and $\|\cdot\|_2$ the Euclidean L_2 norm.

Energy functional We introduce our notation first. Let C be a curve that is the boundary of a set $\omega \subset \Omega$. We denote by Ω_i and Ω_o the inside and the outside of the curve C, respectively. Similar to the piecewise-constant intensity case in image segmentation where the image is assumed to be formed by two regions with distinct intensities values [6], we assume that there are two regions in the image sequence $\{I_n(\cdot)\}_{1\le n\le N}$ whose temporal signals follow closely two different dynamic profiles. We define our energy functional as

$$E(C) = \mu \cdot \mathrm{Length}(C) + \lambda_1 \int_{\Omega_\mathrm{i}} \mathrm{dis}^2(\mathbf{I}(x,y), \bar{\mathbf{I}}^\mathrm{i}) dxdy + \lambda_2 \int_{\Omega_\mathrm{o}} \mathrm{dis}^2(\mathbf{I}(x,y), \bar{\mathbf{I}}^\mathrm{o}) dxdy \tag{5}$$

where $\bar{\mathbf{I}}^\mathrm{i}$ is the average perfusion pattern vector inside the curve C, while $\bar{\mathbf{I}}^\mathrm{o}$ is the average perfusion signal vector outside the curve C. The two distances $\mathrm{dis}^2(\mathbf{I}(x,y), \bar{\mathbf{I}}^\mathrm{i})$ and $\mathrm{dis}^2(\mathbf{I}(x,y), \bar{\mathbf{I}}^\mathrm{o})$ are computed from Equations (3) and (4). The parameters λ_1, λ_2, and μ are positive scalars. The integrals in (5) sum over the pixels, while the distances in the integrands sum over the frames in the sequence.

Segmenting the MRI sequence is now equivalent to minimizing the energy functional (5), as in [3]. In our energy functional, the first term penalizes the total length of the boundary, while the last two terms control the data fidelity. Note that there is no smoothness constraint term because we restrict the estimation to be one single vector $\bar{\mathbf{I}}^\mathrm{i}$ for Ω_i and another vector $\bar{\mathbf{I}}^\mathrm{o}$ for Ω_o. The energy functional (5) is notably distinct from the ones used by other researchers. Not only because the form of its terms is different from usual, but also because it exploits the information available: spatially or intra-image, as well as temporally or across the images in the sequence.

Level set implementation We develop a level set algorithm to minimize the functional (7). The level set method provides an efficient way to handle topological changes. Following for example [6], the level set function $\phi(x,y)$ is defined as follows: $\forall(x,y) \in \Omega_\mathrm{i}, \phi(x,y) > 0; \forall(x,y) \in \Omega_\mathrm{o}, \phi(x,y) < 0; \forall(x,y) \in C, \phi(x,y) = 0$. So, the knowledge of the signs of the level set function $\phi(\cdot)$ is equivalent to segmenting the image. In other words, the level set function $\phi(\cdot)$ implicitly represents the contour C at time t by

$$C = \{(x,y) | \phi(t,x,y) = 0\}. \tag{6}$$

Our algorithm is iterative and we update the estimation of $\bar{\mathbf{I}}^\mathrm{i}$ and of $\bar{\mathbf{I}}^\mathrm{o}$. Lacking space, we expand no further.

3. SEGMENTATION ALGORITHM

Data The experimental data are collected with four groups of rats: 5 normal BN rats, 5 normal DA rats, 6 allograft rats (DA→BN), and 4 isograft rats (BN→BN) were studied. The rats were bolus injected with dextran-coated USPIO particles at a dose of 6 mg Fe/kg of body weight to evaluate first-pass renal perfusion. This dose was experimentally determined to be the most suitable

within a range, see [2]. All rats underwent 128 consecutive snapshot Fast Low Angle SHot (FLASH) coronal dynamic studies in 43 s, on a 4.7-T, 40-cm horizontal bore Bruker AVANCE DRX MR instrument using a 7-cm diameter Bruker volume transceiver coil. The field of view and the section thickness were 6 cm and 2 mm, respectively, and the image matrix was 64×64 pixels. We normalize the signal intensity by the average intensity value on a 3×3-pixel region in the psoas major muscle in the same slice.

Preprocessing Experimentally we observe that the renal perfusion signals at pixels located at the renal cortex are highly correlated with its neighboring pixels, and likewise for the perfusion signals at pixels in the kidney medulla; however, the dynamic signals for pixels on the muscles are uncorrelated noise like. Based on the similarity of the renal perfusion patterns at pixels of the same tissue, and to smooth out some of the variation in these signals, we average the correlation coefficients over a window of the 8 nearest neighbors at each pixel. Let $\mathcal{N}(x,y)$ stand for the 8 nearest neighbors of pixel (x,y), then

$$\bar{c}(x,y) = \frac{1}{8} \sum_{(p,q)\in\mathcal{N}(x,y)} c\left(\mathbf{I}(x,y), \mathbf{I}(p,q)\right) \qquad (7)$$

Thus, we transform the sequence $\{I_n(\cdot)\}_{1\le n\le N}$ into a single image $u(\cdot)$ that captures the correlations of the dynamical signals in the neighborhood at each pixel. Figure 3 (a) displays the image after preprocessing. Note that the pixels located at the kidneys are generally much brighter than the pixels at other organs.

Hierarchical Level set We divide our algorithm into two parts: initialization and segmentation.

Initialization: First we work with the single image $u(\cdot)$ to discard most of the pixels that are not kidney pixels. We develop for this single correlation image a level set algorithm to segment both kidneys. Figure 3 (b) shows as solid contours the curve C^{int} at the end of this initialization part.

Segmentation: We develop a level set algorithm that processes the whole image sequence, but working only with the region inside the curve C^{int} resulting from the initialization stage, see Figure 3 (b); this level set algorithm minimizes now the energy functional in Equation (5). Each iteration is divided into two steps. First, fixing C, find $\bar{\mathbf{I}}^{\text{i}}$ and $\bar{\mathbf{I}}^{\text{o}}$ that minimize the energy functional (5). Second, fixing $\bar{\mathbf{I}}^{\text{i}}$ and $\bar{\mathbf{I}}^{\text{o}}$, find C that minimizes (5). To restrict the evolution of the curve C inside C^{int}, we force the level set function $\phi(t,x,y)$ to be always negative outside the curve C^{int}.

Region-growing With native and transplanted kidneys, to assume that there are only two types of renal perfusion signals in the regions inside C^{int} leads to many errors. To overcome this, we develop a region-growing method to find an approximate solution to the energy functional (5). Our region-growing algorithm is as follows. Initially, each retained pixel is one region in itself. For the pth-region R_p, with N_p pixels, the average temporal sequence is

$$\bar{\mathbf{I}}^p = \frac{1}{N_p} \sum_{(x,y)\in R_p} \mathbf{I}(x,y). \qquad (8)$$

The correlation coefficient $c(p,q)$, computed using Equation (4), quantifies the similarity between the average temporal sequences $\bar{\mathbf{I}}^p$ and $\bar{\mathbf{I}}^q$ of the region R_p and its adjacent neighbor R_q, respectively.

At each iteration of the algorithm, we merge the two neighboring regions with the highest correlation coefficient between their average temporal sequences. That is, we merge the region R_{p^*} with its neighboring region R_{q^*}, such that, (p^*,q^*) maximizes $c(p,q)$. By merging the two regions, we combine the pixels in R_p and R_q into one new region R_{p^*} and delete R_q. At the same time, all the neighbors of R_p and R_q become the neighbors of R_{p^*}. Finally, the average temporal sequence for the new region R_{p^*} is calculated by the weighted sum

$$\bar{\mathbf{I}}^{p^*} = \frac{N_p}{N_p+N_q}\bar{\mathbf{I}}^p + \frac{N_q}{N_p+N_q}\bar{\mathbf{I}}^q \qquad (9)$$

The correlation coefficients of the regions affected by the merging are also updated. The algorithm continues and a new iteration restarts until the maximum correlation coefficient is below a certain threshold α. We chose $\alpha = 0.90$ in this study. Thus, the region inside C^{int} is divided into several regions with different sizes. Among the rats we studied, the first two largest regions are the cortex of the left and of the right kidneys.

4. EXPERIMENTAL RESULTS

We applied the level set segmentation method described in section 3 to normal BN rats to extract the renal cortex from USPIO-enhanced dynamic MR image sequences. In our experiments, we chose the parameters as follows: $\lambda_1 = \lambda_2 = 2500$, and $\mu = 80$. Figure 3 shows the segmentation results at the end of each part of our level set algorithm for one of the BN rats. In Figures 3 (b)and (c), the initial assumed contours are the circles (dotted lines), and the solid contours are the final results of Parts 1 and 2, respectively. Figure 3 (d) shows the extracted cortex by combining the segmentation results from Figures 3 (b) and (c).

We also applied the region-growing algorithm presented in section 3 to 4 isograft rats and 6 allograft rats. We illustrate its segmentation performance for one isograft rat and one allograft rat in Figures 4 (a) and (b), respectively. We plot the first two largest regions. The stars label the cortex of the right (native)

kidneys, while the circles label the cortex of the left (transplanted) kidneys. As shown, the first two largest regions are the cortex of the left and the right kidneys.

The results in Figures 3 and 4 indicate that the cortex is the most homogeneous region in terms of the first-pass renal perfusion signal. The automatic segmentation results of the cortex were validated by experts that showed that they are highly consistent with their manual segmentations. With the cortex automatically extracted, we can apply to each pixel the geometric based statistical analysis we proposed in [2] to detect possible graft rejection rather than using an average signal over a few manually selected pixels as in [2]. This reliability for early detection of organ rejection that this provides is the theme of future investigations.

In conclusion we describe an energy-based segmentation algorithm that has successfully extracted the cortex without user intervention. Our experimental results with 10 normal rats and 10 transplanted rats have shown that the algorithm performs very well. USPIO-enhanced dynamic MRI is a powerful methodology in the study of kidney transplant rejection. Our long-term objectives are to develop automatic segmentation tools that can extract the cortex and the medulla from the MRI sequence, and that can automatically detect patterns of abnormal behavior of the transplanted kidneys and provide a quantitative measure of their degree of rejection.

Fig. 1. USPIO-enhanced dynamic MRI sequence

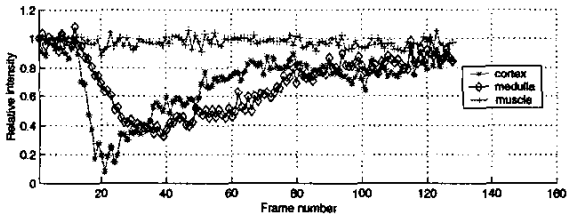

Fig. 2. Normalized renal perfusion signals.

5. REFERENCES

[1] Y. Sun, D. Yang, Q. Ye, C. Ho, and J. M. F. Moura, "A Novel Approach in Analyzing Dynamic Intrarenal Signals Using USPIO and MRI," 9th ISMRM/ESMRMB Joint Annual Meeting, Glasgow, Scotland, April 2001.

[2] D. Yang, Q. Ye, M. Williams, Y. Sun, T. Hu, D. Williams, J. M. F. Moura, and C. Ho,"USPIO-Enhanced Dynamic MRI: Evaluation of Normal and Transplanted Rat Kidneys," J. Magnetic Resonance in Medicine,46:1152-1163, 2001.

[3] D. Mumford and J. Shah, "Optimal Approximation by Piecewise Smooth Functions and Associated variational Problems," Comm. Pure Appl. Math, Vol.42, 577-685, 1989.

[4] Pedro M. Q. Aguiar and J. M. F. Moura, "Maximum Likelihood Estimation of the Template of a Rigid Moving Object," EMMCVPR'01, Energy Min. Methods in Comp. Vision and Pattern Recognition, Springer Verlag, July, 1999.

[5] I. Gohberg, P. Lancaster, and L. Rodman, "Invariant Subspaces of Matrices with Applications," John Wiley and Sons, 1986.

[6] T. F. Chan and L. A. Vese, "Active Contour Without Edges," IEEE Trans. Image Processing, Vol.10:(2), 266-277, 2001.

[7] G. H. Golub and C. F. Van Loan, "Matrix Computations," Baltimore: Johns Hopkins University Press, pp.75-79 1996.

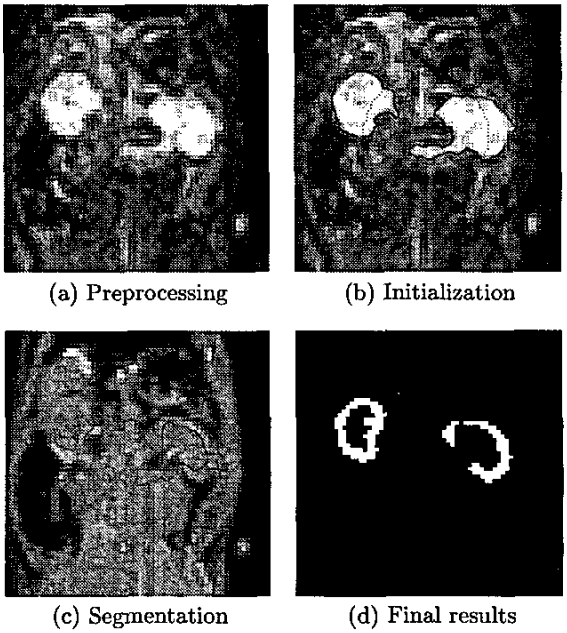

(a) Preprocessing (b) Initialization

(c) Segmentation (d) Final results

Fig. 3. Segmentation results of a normal BN rat.

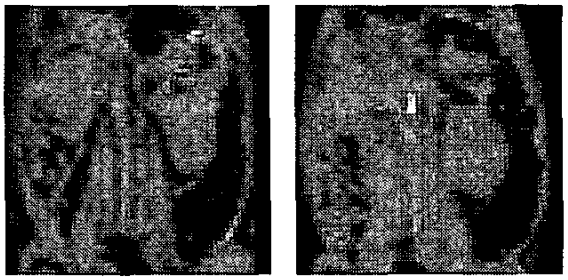

(a) Isograft (b) Allograft

Fig. 4. Segmentation results for transplanted rats.